Magnetic polarization in the optical absorption of metallic nanoparticles

A. Asenjo-Garcia,* A. Manjavacas, V. Myroshnychenko, and F. J. García de Abajo

Instituto de Química Física Rocasolano - CSIC, Serrano 119, 28006 Madrid, Spain

* *ana.asenjo@csic.es*

Abstract: We find remarkably strong absorption due to magnetic polarization in common colloidal and lithographic metallic nanoparticles. Our analysis is based upon a thorough examination of the dipolar electric and magnetic polarizabilities for representative combinations of nanoparticle composition, size, and morphology. We illustrate this concept by first discussing absorption in metallic spheres and then exploring ellipsoids, disks, and rings. Magnetic polarization reaches $\sim 90\%$ of the total absorption in 100 nm disks and rings for wavelengths above $1\,\mu$m under co-linear electric and magnetic irradiation. Our results demonstrate that the magnetic contribution to absorption cannot be naively overlooked, as it can largely exceed the contribution of electric polarization.

OCIS codes: (250.5403) Plasmonics; (240.6680) Surface plasmons; (290.4020) Mie theory.

References and links

1. L. Novotny and B. Hecht, *Principles of Nano-Optics* (Cambridge University Press, New York, 2006).
2. V. Myroshnychenko, J. Rodríguez-Fernández, I. Pastoriza-Santos, A. M. Funston, C. Novo, P. Mulvaney, L. M. Liz-Marzán, and F. J. García de Abajo, "Modelling the optical response of gold nanoparticles," Chem. Soc. Rev. **37**, 1792–1805 (2008).
3. H. A. Atwater and A. Polman, "Plasmonics for improved photovoltaic devices," Nat. Mater. **9**, 205–213 (2010).
4. D. P. O'Neal, L. R. Hirsch, N. J. Halas, J. D. Payne, and J. L. West, "Photo-thermal tumor ablation in mice using near infrared-absorbing nanoparticles," Cancer Lett. **209**, 171–176 (2004).
5. C. Loo, A. Lowery, N. J. Halas, J. L. West, and R. Drezek, "Inmunotargeted nanoshells for integrated cancer imaging and therapy," Nano Lett. **5**, 709–711 (2005).
6. J. H. Lee, J. Jang, J. Choi, S. H. Moon, S. Noh, J. Kim, J. Kim, I. S. Kim, K. I. Park, and J. Cheon, "Exchange-coupled magnetic nanoparticles for efficient heat induction," Nat. Nanotech. **6**, 418–422 (2011).
7. H. Huang, S. Delikanli, H. Zeng, D. M. Ferkey, and A. Pralle, "Remote control of ion channels and neurons through magnetic-field heating of nanoparticles," Nat. Nanotech. **5**, 602–606 (2010).
8. M. S. Yavuz, Y. Cheng, J. Chen, C. M. Cobley, Q. Zhang, M. Rycenga, J. Xie, C. Kim, K. H. Song, A. G. Schwartz, L. V. Wang, and Y. Xia, "Gold nanocages covered by smart polymers for controlled release with near-infrared light," Nat. Mater. **8**, 935–939 (2009).
9. M. W. Knight, H. Sobhani, P. Nordlander, and N. J. Halas, "Photodetection with active optical antennas," Science **332**, 702–704 (2011).
10. L. Genzel and U. Kreibig, "Dielectric function and infrared absorption of small metal particles," Z. Physik B **37**, 93–101 (1980).
11. M. Wilkinson, B. Mehlig, and P. N. Walker, "Magnetic dipole absorption of radiation in small conducting particles," J. Phys. Condens. Matter **10**, 2739–2758 (1998).
12. P. M. Tomchuk and N. I. Grigorchuk, "Shape and size effects on the energy absorption by small metallic particles," Phys. Rev. B **73**, 155423 (2006).
13. N. I. Grigorchuk and P. M. Tomchuk, "Theory for absorption of ultrashort laser pulses by spheroidal metallic nanoparticles," Phys. Rev. B **80**, 155456 (2009).

#177151 - $15.00 USD Received 2 Oct 2012; revised 8 Nov 2012; accepted 12 Nov 2012; published 4 Dec 2012

14. A. García-Etxarri, R. Gómez-Medina, L. S. Froufe-Pérez, C. López, L. Chantada, E. Scheffold, J. Aizpurua, M. Nieto-Vesperinas, and J. J. Sáenz, "Strong magnetic response of submicron silicon particles in the infrared," Opt. Express **19**, 4815–4826 (2011).
15. T. A. Evans and J. K. Furdyna, "Microwave magnetic dipole interaction in small InSb spheres: induced cyclotron-resonance-like absorption in the Rayleigh limit," Phys. Rev. B **8**, 1461–1476 (1973).
16. P. O. Chapuis, M. Laroche, S. Volz, and J. J. Greffet, "Near-field induction heating of metallic nanoparticles due to infrared magnetic dipole contribution," Phys. Rev. B **77**, 125402 (2008).
17. P. O. Chapuis, M. Laroche, S. Volz, and J. J. Greffet, "Radiative heat transfer between metallic nanoparticles," Appl. Phys. Lett. **93**, 201906 (2008).
18. A. Manjavacas and F. J. García de Abajo, "Radiative heat transfer between neighboring particles," Phys. Rev. B **86**, 075466 (2012).
19. A. Manjavacas and F. J. García de Abajo, "Thermal and vacuum friction acting on rotating particles," Phys. Rev. A **82**, 063827 (2010).
20. S. Vignolini, F. Intonti, F. Riboli, L. Balet, L. H. Li, M. Francardi, A. Gerardino, A. Fiore, D. S. Wiersma, and M. Gurioli, "Magnetic imaging in photonic crystal microcavities," Phys. Rev. Lett. **105**, 123902 (2010).
21. M. Burresi, T. Kampfrath, D. van Osten, J. C. Prangsma, B. S. Song, S. Noda, and L. Kuipers, "Magnetic light-matter interactions in photonics crystal nanocavity," Phys. Rev. Lett. **105**, 123901 (2010).
22. H. W. Kihm, S. M. Koo, Q. H. Kim, K. Bao, J. E. Kihm, W. S. Bak, S. H. Eah, C. Lienau, H. Kim, P. Nordlander, N. J. Halas, N. K. Park, and D. S. Kim, "Bethe-hole polarization analyser for the magnetic vector of light," Nat. Commun. **2**, 451 (2011).
23. S. Karaveli and R. Zia, "Strong enhancement of magnetic dipole emission in a multilevel electronic system," Opt. Lett. **35**, 3318–3320 (2010).
24. S. Karaveli and R. Zia, "Spectral tuning by selective enhancement of electric and magnetic dipole emission," Phys. Rev. Lett. **106**, 193004 (2011).
25. L. Shi, E. Xifré-Pérez, F. J. García de Abajo, and F. Meseguer, "Looking through the mirror: Optical microcavity-mirror image photonic interaction," Opt. Express **20**, 11247–11255 (2012).
26. E. J. Zeman and G. C. Schatz, "An accurate electromagnetic theory study of surface enhancement factors for silver, gold, copper, lithium, sodium, aluminum, gallium, zinc, and cadmium," J. Phys. Chem. **91**, 634–643 (1987).
27. P. B. Johnson and R. W. Christy, "Optical constants of the noble metals," Phys. Rev. B **6**, 4370–4379 (1972).
28. H. C. van de Hulst, *Light Scattering by Small Particles* (Dover, New York, 1981).
29. G. Mie, "Beiträge zur optik trüber medien, speziell kolloidaler metallösungen," Ann. Phys. (Leipzig) **25**, 377–445 (1908).
30. N. W. Ashcroft and N. D. Mermin, *Solid State Physics* (Harcourt College Publishers, New York, 1976).
31. F. J. García de Abajo and A. Howie, "Relativistic electron energy loss and electron-induced photon emission in inhomogeneous dielectrics," Phys. Rev. Lett. **80**, 5180–5183 (1998).
32. Zhang, J.; MacDonald K. F.; Zheludev, N. I. arXiv:1203.6110v1.
33. G. Baffou, R. Quidant, and F. J. García de Abajo, "Nanoscale control of optical heating in complex plasmonic systems," ACS Nano **4**, 709–716 (2010).
34. A. G. Curto, G. Volpe, T. H. Taminiau, M. P. Kreuzer, R. Quidant, and N. F. van Hulst, "Unidirectional emission of a quantum dot coupled to a nanoantenna," Science **329**, 930–933 (2010).

1. Introduction

The understanding of optical absorption in areas as diverse as atomic physics, solid state physics, and electromagnetism has committed a large deal of work that is currently flourishing in the field of nanoplasmonics. Light absorption by metallic nanoparticles is mainly mediated by the excitation of valence and conduction electrons as well as their collective oscillations at visible and near-infrared (vis-NIR) frequencies known as surface plasmons [1, 2]. Besides its fundamental interest, nanoplasmonics finds a wide range of applications ranging from photovoltaic devices [3] to biomedicine (e.g., photothermal tumor ablation [4–6], remote control of ion channels in cells [7], and drug delivery [8]). In this context, plasmon-assisted absorption opens additional avenues for photodetection and spectroscopy applications [9] and can be a source of unexpected phenomena, such as the dominant magnetic absorption here investigated.

Absorption due to electric polarization has been extensively studied in the past, while its magnetic counterpart is generally regarded as a weak contribution and has only been addressed for spherical and ellipsoidal particles [10–14]. However, there are several relevant situations in which the magnetic contribution to absorption can even exceed the electric contribution,

#177151 - $15.00 USD Received 2 Oct 2012; revised 8 Nov 2012; accepted 12 Nov 2012; published 4 Dec 2012

specifically in particles of high aspect ratio made of a well conducting metal, as we show below. This is the result of non-resonant magnetic polarization that produces eddy currents induced by the time-varying magnetic field [15], just in the same way as electric absorption arises from the currents needed to establish an electric polarization in the particle. Eddy currents generate Joule heating and produce forces commonly used for levitating and braking metallic objects. Magnetic dissipation is also relevant to correctly describe dispersion forces, including the Casimir effect and radiative heat transfer between non-ideal conductors [16–18], as well as quantum friction [19]. Recently, the magnetic response has been realized to be an important element in the description of the near field in nanostructured environments, where it has been recently measured at optical frequencies [20–22] and used to enhance magnetic dipole emission in electronic systems [23,24]. In high-permittivity colloids, the fundamental Mie mode has been shown to produce a prominent, well-defined magnetic dipole [14], which has been predicted to give rise to optical repulsion from a metal surface [25].

Here, we report large magnetic response exceeding the electric response in common metallic nanoparticles within the near infrared. We compare the electric and magnetic dipolar polarizabilities of metallic spheres, ellipsoids, disks, and rings of different size, aspect ratio, and composition. Particles are described via their frequency-dependent dielectric function, and their optical response is obtained by rigorously solving Maxwell's equations in the presence of incident light. The magnetic contribution is found to dominate the absorption for metals of large conductivity at moderate particle size, specially in particles of high aspect ratio.

2. Magnetic absorption in spheres

During absorption, the incoming photons generate real excitations in the particles. The absorption density is proportional to the local electric-field intensity multiplied by the imaginary part of the dielectric function. This emerges in the particle polarizability α through an imaginary part in excess of the value that is found in non-absorbing particles (i.e., $\mathrm{Im}\{\alpha\} \geq 2\sqrt{\varepsilon_h}k^3|\alpha|^2/3$, where $k=\omega/c$ is the light wave vector and ε_h is the permittivity of the surrounding host medium [28]). We focus first on homogeneous spheres, for which closed-form expressions of the polarizability are readily available within Mie scattering theory [28, 29].

We consider a spherical nanoparticle of small radius R compared to the wavelength inside the host medium, where $\lambda = 2\pi/k$ is the free-space light wavelength, so that the dipolar response is dominant. In vacuum, the electric and magnetic dipolar polarizabilities of the particle can then be expressed as [2]

$$\alpha_E = \frac{3}{2}\frac{1}{k^3}t_1^E, \tag{1a}$$

$$\alpha_M = \frac{3}{2}\frac{1}{k^3}t_1^M, \tag{1b}$$

in terms of the corresponding dipolar Mie coefficients

$$t_1^E = \frac{j_1(\rho)\,[\rho_m j_1(\rho_m)]' + \varepsilon_m j_1(\rho_m)\,[\rho\, j_1(\rho)]'}{h_1^{(+)}(\rho)\,[\rho_m j_1(\rho_m)]' - \varepsilon_m j_1(\rho_m)\left[\rho h_1^{(+)}(\rho)\right]'}, \tag{2a}$$

$$t_1^M = \frac{-\rho_m j_1(\rho)\,[j_1(\rho_m)]' + \rho\, j_1(\rho_m)\,[j_1(\rho)]'}{\rho_m h_1^{(+)}(\rho)\,[j_1(\rho_m)]' - \rho\, j_1(\rho_m)\left[h_1^{(+)}(\rho)\right]'}, \tag{2b}$$

where ε_m is the metal dielectric function inside the particle, $\rho_m = \sqrt{\varepsilon_m}kR$, $\rho = kR$, $h_1^{(+)} = ih_1^{(1)}$, and the primes indicate differentiation of the spherical Bessel and Hankel functions j_1 and $h_1^{(+)}$ with respect to their arguments.

#177151 - $15.00 USD Received 2 Oct 2012; revised 8 Nov 2012; accepted 12 Nov 2012; published 4 Dec 2012

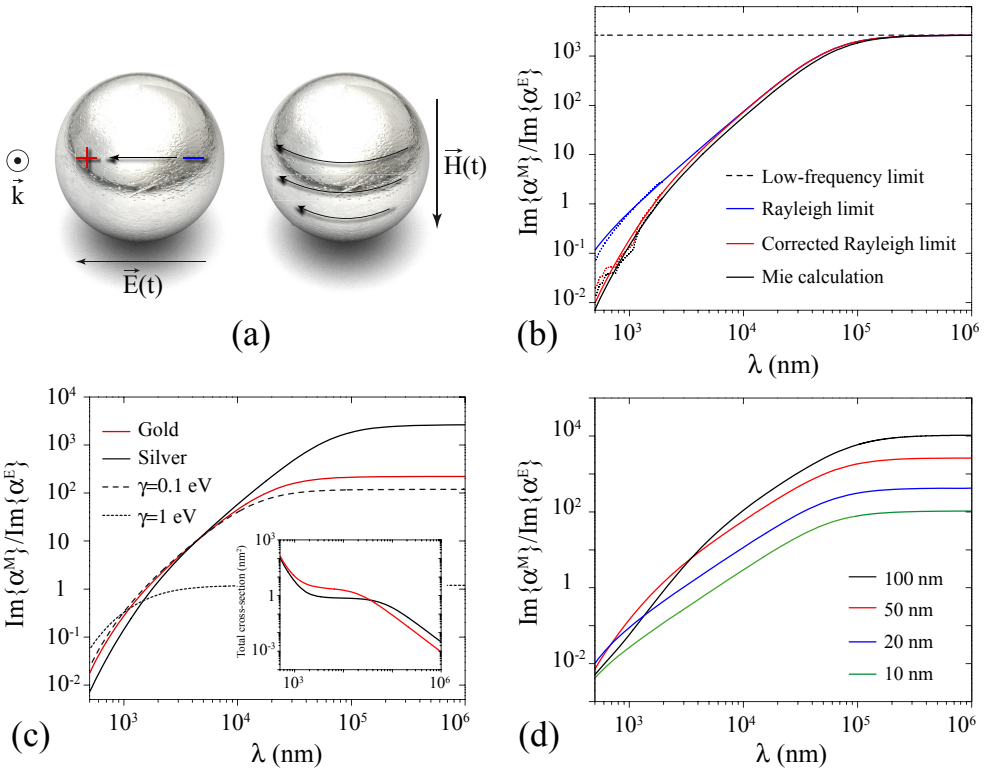

Fig. 1. Electric vs magnetic absorption in metallic nanospheres. (a) Schematic representation of induced currents leading to electric and magnetic absorption, respectively. (b) Ratio between the imaginary parts of the magnetic and the electric polarizabilities for a 50 nm silver sphere. Exact Mie theory (black solid curve) is compared to various approximations, as explained in the text. Solid curves correspond to a Drude-like dielectric function with $\omega_p = 9.04\,\mathrm{eV}$ and $\gamma = 0.021\,\mathrm{eV}$ [26], while dotted curves are obtained from the tabulated dielectric function of silver [27]. (c) Conductivity dependence of the magnetic-to-electric absorption ratio for 50 nm spheres described by a Drude dielectric function with parameters appropriate to gold ($\omega_p = 8.89\,\mathrm{eV}$ and $\gamma = 0.071\,\mathrm{eV}$ [26]) and silver ($\omega_p = 9.04\,\mathrm{eV}$ and $\gamma = 0.021\,\mathrm{eV}$ [26]), compared to more lossy particles (broken curves, obtained with increased damping γ and similar plasma frequency). (d) Size dependence for silver spheres described by the Drude dielectric function.

#177151 - $15.00 USD Received 2 Oct 2012; revised 8 Nov 2012; accepted 12 Nov 2012; published 4 Dec 2012

Interestingly, in the quasistatic (Rayleigh) limit ($|\rho_m|, |\rho| << 1$), Eq. (1) reduces to

$$\alpha_E = R^3 \frac{\varepsilon_m - 1}{\varepsilon_m + 2}, \tag{3a}$$

$$\alpha_M = R^3 \left(\frac{R}{\lambda}\right)^2 \frac{2\pi^2}{15} \left[\varepsilon_m - 1\right], \tag{3b}$$

and hence the magnetic part appears to be $\sim (R/\lambda)^2$ times smaller than the electric part: electric dipoles are expected to dominate over magnetic ones. We can easily show that this is not true even for spherical particles orders of magnitude smaller than the wavelength. The key point is that absorption is proportional to the imaginary part of the polarizabities, and thus, the ratio between magnetic and electric contributions to absorption is simply given by $\mathrm{Im}\{\alpha_M\}/\mathrm{Im}\{\alpha_E\}$.

At small frequencies below interband transitions in noble metals, it is useful to approximate ε_m by the Drude dielectric function [30]

$$\varepsilon_m = 1 - \frac{\omega_p^2}{\omega(\omega + i\gamma)}, \tag{4}$$

where ω_p and γ are the bulk plasmon frequency and damping-rate, respectively. Inserting Eq. (4) into Eq. (3), we find

$$\frac{\mathrm{Im}\{\alpha_M\}}{\mathrm{Im}\{\alpha_E\}} \longrightarrow \frac{1}{90}\left(\frac{R}{c}\right)^2 \left(\frac{\omega_p^2}{\gamma}\right)^2 = \frac{8\pi^2}{45}\left(\frac{R\sigma_0}{c}\right)^2 \tag{5}$$

in the $\omega << \gamma, \omega_p$ limit, where we have introduced the static conductivity $\sigma_0 = \omega_p^2/4\pi\gamma$. Clearly, magnetic absorption can dominate if $R\sigma_0/c$ is sufficiently large. In particular, as we show in Fig. 1(b), the high conductivity of silver (for Drude parameters $\omega_p = 9.04\,\mathrm{eV}$ and $\gamma = 0.021\,\mathrm{eV}$ [26]) leads to huge values of this ratio in small 50 nm particles (dashed line), although this result is only valid at long wavelengths. The ratio decreases at smaller wavelengths, but still remains above 1 in the IR part of the spectrum. Incidentally, the Drude model produces a satisfactory description of absorption down to the vis-NIR (Fig. 1(b), solid curves), compared with a measured dielectric function [27] (dotted curves). However, the Rayleigh limit (Eq. (3), blue curves) overestimates the magnetic contribution in that spectral region compared to Mie theory (Eq. (1) and Eq. (2), black curves) because the skin depth (~ 25 nm in silver over the vis-NIR) becomes comparable to the particle radius. These effects arise from retardation in the electric polarizability, which we can incorporate to first order through the substitution $\alpha_E \to 1/(\alpha_E^{-1} - 2ik^3/3)$. The result of this correction (without modifying α_M) agrees rather well with Mie theory over the spectral region under consideration (Fig. 1(b), red curve).

Figure 1(c) clearly points out that an increase in damping rate (i.e., a decrease in conductivity) reduces the relative role of magnetic absorption, while Fig. 1(d) shows that magnetic absorption increases with particle size (like in the limit of Eq. (5)). Both of these results are consistent with the interpretation in terms of eddy currents.

3. Influence of particle shape on the fraction of magnetic absorption

We are interested in the relative role of magnetic absorption produced by anisotropy in non-spherical particles. Figures 2(d)-2(i) shows the relative magnetic contribution in ellipsoids, disks, and rings obtained from boundary-element-method (BEM) electromagnetic simulations [31]. The polarizabilities are obtained from the numerically calculated scattering matrix using Eq. (1). We normalize the magnetic absorption to the sum of electric and magnetic absorptions for polarization directions as driven by incident plane-wave light (see insets). The absorption cross-section takes large values exceeding the particle geometrical cross-section around

#177151 - $15.00 USD Received 2 Oct 2012; revised 8 Nov 2012; accepted 12 Nov 2012; published 4 Dec 2012

the plasmonic resonances in the vis-NIR (Figs. 2(a)-2(c)). At longer wavelengths, absorption shows a monotonic decrease. Simultaneously, the relative contribution of magnetic absorption takes over as the wavelength increases. These trends are the same as in spheres, but anisotropy produces two important effects: (i) it displaces the Mie dipole-plasmon resonance to the red with respect to the sphere; and (ii) it strongly modifies the relative contribution of magnetic absorption. As a rule, magnetic absorption increases with respect to its relative value in spheres when the electric field is directed along a narrower direction of the particle. For example, in elongated ellipsoids with incidence along a direction normal to the symmetry axis, magnetic absorption is strongly suppressed when the electric field is along that axis (Fig. 2(d)), which indicates the presence of strong electric polarization along the long direction of the particle (Fig. 2(a)). In contrast, when the electric field is across the symmetry axis (Fig. 2(g) and Fig. 5(a-bottom)), the magnetic field creates strong currents circling the ellipsoid, which increase the relative contribution of magnetic absorption. Interestingly, when thinning a sphere to produce an elongated ellipsoid, magnetic absorption is first increasing under these illumination conditions and eventually decreases below the level of spheres (see appendix). Similar conclusions can be extracted for disks and rings.

As expected, the cross section of Figs. 2(a)-2(c), obtained with full inclusion of all multipoles via BEM, are nearly identical to the one obtained from the dipolar contribution via the well-known expression $4\pi k\mathrm{Im}\{\alpha_E+\alpha_M\}$, thus corroborating the validity of the dipole approximation in the present analysis.

We further consider illumination under two in-phase, counter-propagating, orthogonally polarized light beams, which produce mutually aligned total electric and magnetic fields [22]. This provides a fair comparison of the relative importance of electric and magnetic polarization along a common direction, which we take along the symmetry axis of the particle. Figure 3 shows that the magnetic contribution to the total absorption is remarkably high, reaching 90% in the NIR for disks and rings. Even at 500 nm, the magnetic contribution is as high as 30%. Under this configuration, the electric field produces only a small dipole perpendicular to the disk (ring), whereas the magnetic field is optimally oriented to create eddy currents circling the disk (ring) perimeter, and thus maximizing the relative contribution of magnetic absorption.

The two-counter-propagating-beam configuration allows us to illuminate the particle with arbitrary values and orientations of the electric and magnetic fields in the plane perpendicular to the directions of propagation. In particular, it is possible to just have pure electric or magnetic polarization. This possibility is illustrated in Fig. 4 for both axial and radial orientations of the field. We define the cross section for two beams as an extension of the single-plane illumination case: the absorbed power divided by the total incident light intensity, assuming equally intense beams. The cross section is then obtained from the expression $(\lambda/2)|\mathbf{E}_1^{\mathrm{ext}}+\mathbf{E}_2^{\mathrm{ext}}|^{-2}\sum_j \mathrm{Im}\{\mathbf{f}_j\cdot(\mathbf{E}_j^{\mathrm{ext}})^*\}$, where $j=1,2$ runs over the two far-field beam directions and $\mathbf{f}$ is the far-field electric amplitude. We compared fully numerical results (Fig. 4, solid curves) to semi-analytical expressions (broken curves) for $\mathbf{f}$ in terms of the polarizability, which are in turn extracted as explained above. The largest values of the cross section are obtained under pure radial electric-field illumination, with values well above the disk area in the spectral region of the symmetric plasmon resonance around 700 nm. Large values of the magnetic absorption are also obtained under axial magnetic illumination. This configuration can actually be used to modulate the absorbed power by rotating the polarization vector of the incident beams, in a way similar to what has been recently reported for thin metamaterial structures [32]. A practical implementation of magnetic absorption with a single beam is also possible by depositing the nanoparticle on metal surface such as gold, whose reflectivity above 1000 nm wavelength is close to 100% because the parallel electric field is nearly canceled near the surface, while the amplitude of the magnetic field is doubled.

#177151 - $15.00 USD Received 2 Oct 2012; revised 8 Nov 2012; accepted 12 Nov 2012; published 4 Dec 2012

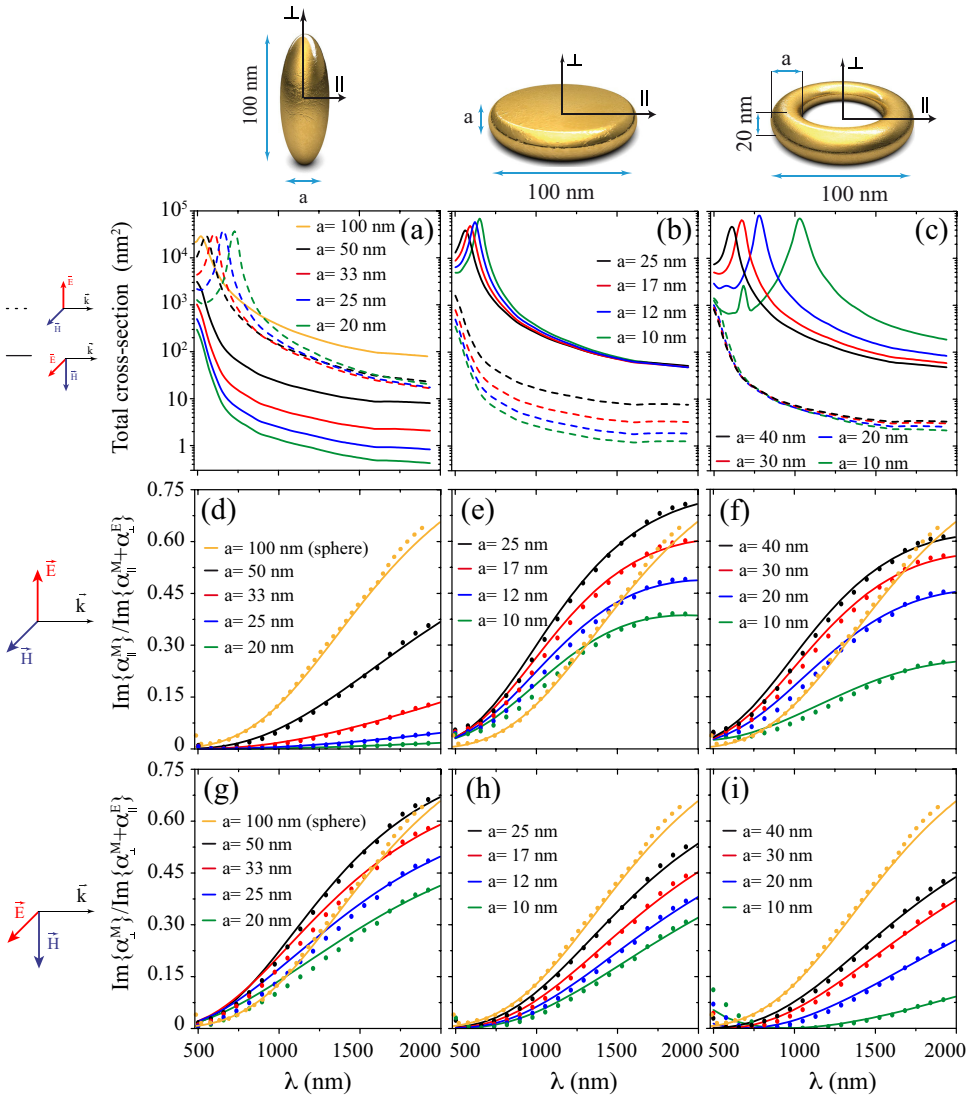

Fig. 2. Spectral dependence of the magnetic contribution to absorption for gold particles of different shape and aspect ratio: (a,d,g) ellipsoids, (b,e,h) rounded disks, and (c,f,i) rings. (a)-(c) Absorption cross-section for two different orientations of the incident electric and magnetic fields relative to the particle symmetry axis (see insets in (a)) and different particle sizes (see upper insets). (d)-(i) Fraction of magnetic losses. Solid curves in (d)-(i) are obtained using a Drude permittivity for gold, while the rest of calculations use tabulated optical data [27]. Parallel and perpendicular orientations in the polarization components are referred to the direction of **k**.

#177151 - $15.00 USD Received 2 Oct 2012; revised 8 Nov 2012; accepted 12 Nov 2012; published 4 Dec 2012

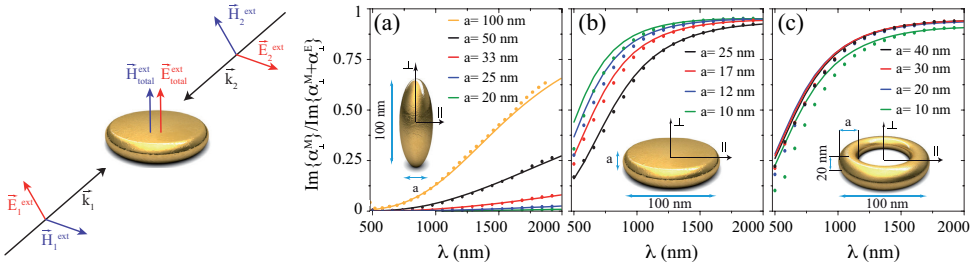

Fig. 3. Magnetic absorption under co-linear illumination conditions. We consider two counter-propagating beams, as shown in the left inset, giving rise to aligned external electric and magnetic fields [22]. The spectral dependence of the magnetic contribution to absorption is shown in (a)-(c) for gold ellipsoids, disks, and rings, with the external fields along the axial direction of symmetry. Solid curves and symbols are obtained using the Drude model for gold and a measured dielectric function [27], respectively.

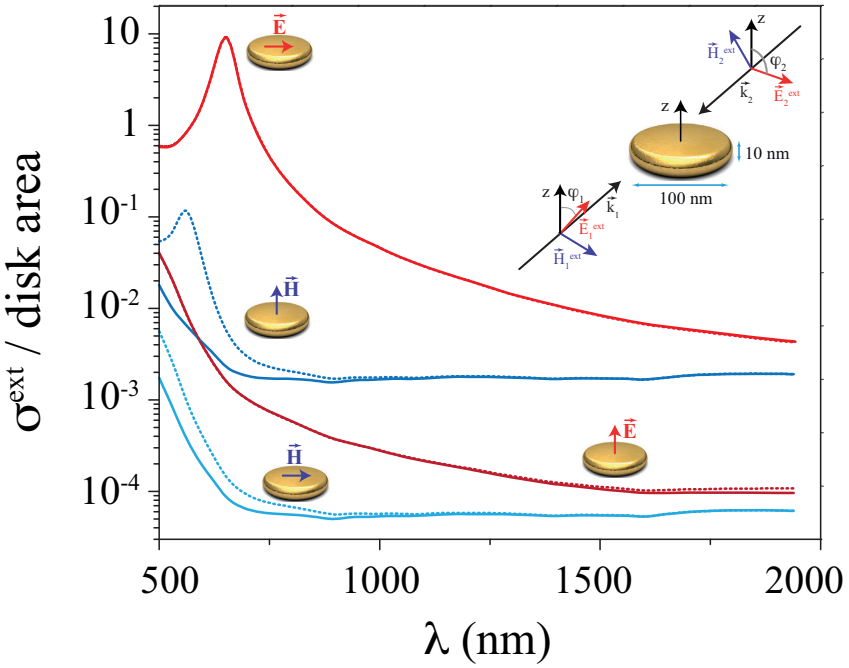

Fig. 4. Electric and magnetic extinction by a gold nanodisk. We consider two counter-propagating beams, as shown in the inset, leading to only electric or magnetic non-vanishing external field components at the center of the particle. Specifically, we take $(\varphi_1, \varphi_2) = (0, 0)$ for axial **E**; $(\pi/2, \pi/2)$ for radial **E**; $(-\pi/2, \pi/2)$ for axial **H**; and $(0, \pi)$ for radial **H** (see insets). Semi-analytical (broken curves) and fully numerical (solid curves) calculations are compared (see text).

#177151 - $15.00 USD Received 2 Oct 2012; revised 8 Nov 2012; accepted 12 Nov 2012; published 4 Dec 2012

4. Conclusion

In summary, we have shown that the absorption properties of common metal nanoparticles extensively used in plasmonics is unexpectedly driven by the magnetic dipole component in the vis-NIR part of the spectrum. The magnetic contribution can be understood as arising from dissipation of eddy currents produced by the temporal variation of the magnetic field, which takes place at frequencies above the plasmonic resonances and is strongly dependent on size, morphology, and composition. Large metal conductivities favor a dominant magnetic absorption. Magnetic absorption also depends on particle shape and is comparatively higher when the electric field is oriented along a narrower direction of the particles, thus minimizing the degree of electric polarization. For example, in elongated ellipsoids and flat disks of 1:2 and 1:4 aspect ratio, respectively, magnetic absorption is dominant at wavelengths above $\sim 1300\,\text{nm}$. Under illumination with co-linear electric and magnetic fields, magnetic absorption reaches 90% of the total absorption. Our work provides a comprehensive understanding of optical absorption in metallic particles that should be relevant to control heat deposition in the context of thermoplasmonics [33], heat dissipation through radiative heat transfer [16, 17], and light emission exhibiting spatial patterns associated with magnetic modes [23, 24, 34].

Appendix

We provide in Fig. 5 and Fig. 6 calculations of the relative contribution of magnetic absorption in anisotropic silver particles of sizes and shapes similar to the gold nanoparticles considered in the main text.

Additionally, we provide calculations for gold and silver ellipsoids in Fig. 7 and Fig. 8, respectively, under illumination with a beam along the symmetry axis. Interestingly, elongated ellipsoids produce a high relative contribution of magnetic absorption compared to the sphere, particularly in the vis-NIR region, which yields magnetic absorption dominant in ellipsoids of aspect ratio 1:2 above a wavelength of $\sim 1300\,\text{nm}$ for gold and $\sim 1500\,\text{nm}$ for silver.

#177151 - $15.00 USD Received 2 Oct 2012; revised 8 Nov 2012; accepted 12 Nov 2012; published 4 Dec 2012

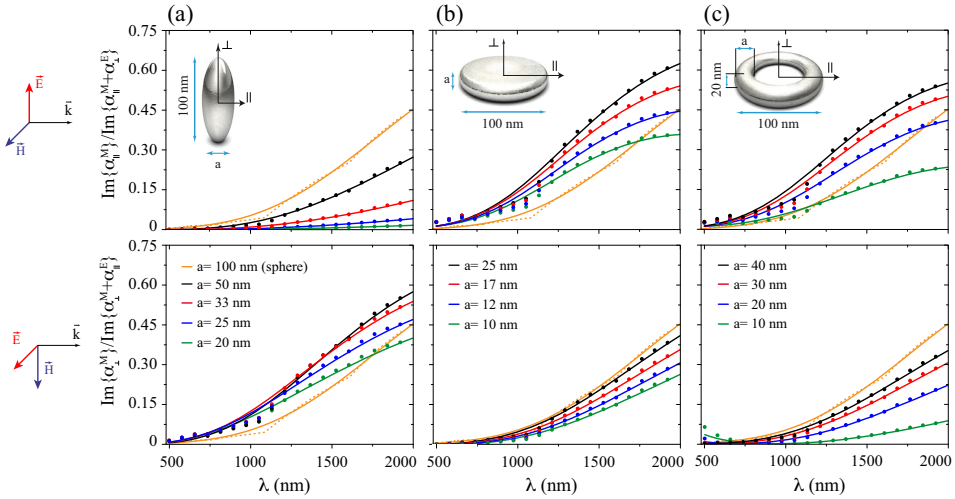

Fig. 5. Same as Fig. 2 of the main paper for silver particles. The figure shows the spectral dependence of the magnetic contribution to absorption for silver particles of different shape and aspect ratio: (a) ellipsoids, (b) rounded disks, and (c) rings. Two different orientations of the incident electric and magnetic fields are considered (see left insets). Solid curves are obtained using a Drude permittivity for silver, while the rest of calculations use tabulated optical data [27].

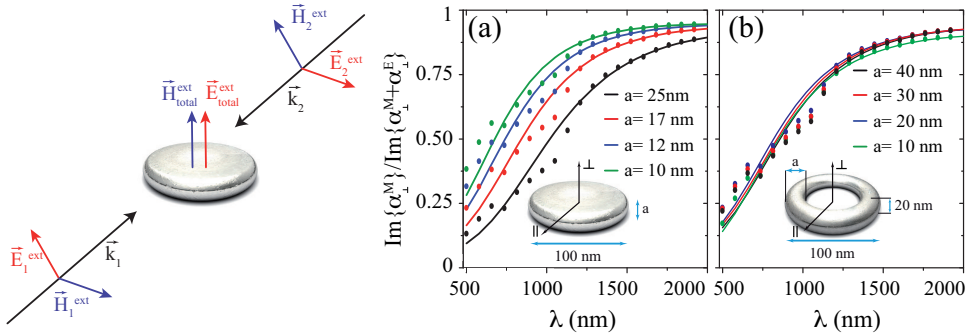

Fig. 6. Same as Fig. 3 of the main paper for silver particles. The figure illustrates the magnetic absorption under co-linear illumination conditions (see left inset). The spectral dependence of the magnetic contribution to absorption is shown in (a), (b) for silver disks and rings, with the external fields along the axial direction of symmetry. Solid curves and symbols are obtained using the Drude model for silver and a measured dielectric function [27], respectively.

#177151 - $15.00 USD Received 2 Oct 2012; revised 8 Nov 2012; accepted 12 Nov 2012; published 4 Dec 2012

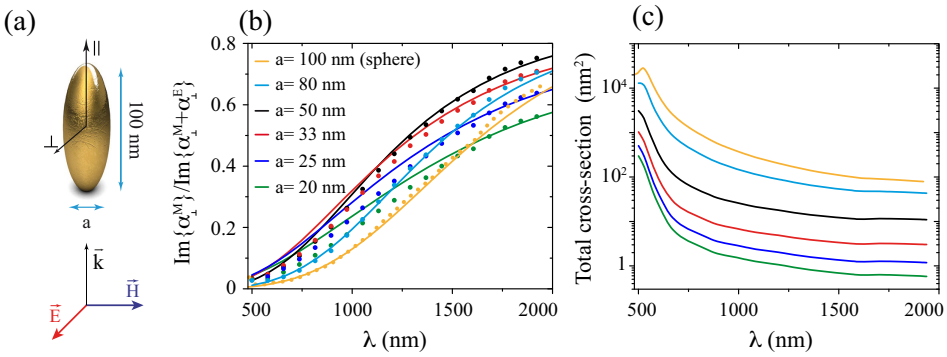

Fig. 7. Relative contribution of magnetic absorption for gold ellipsoids and light incidence along the axis of symmetry. (a) Sketch of the geometry. (b) Fraction of magnetic absorption. (c) Absorption cross-section. A Drude permittivity for gold is used in the solid curves of (b) and a tabulated dielectric function [27] for the rest of the calculations.

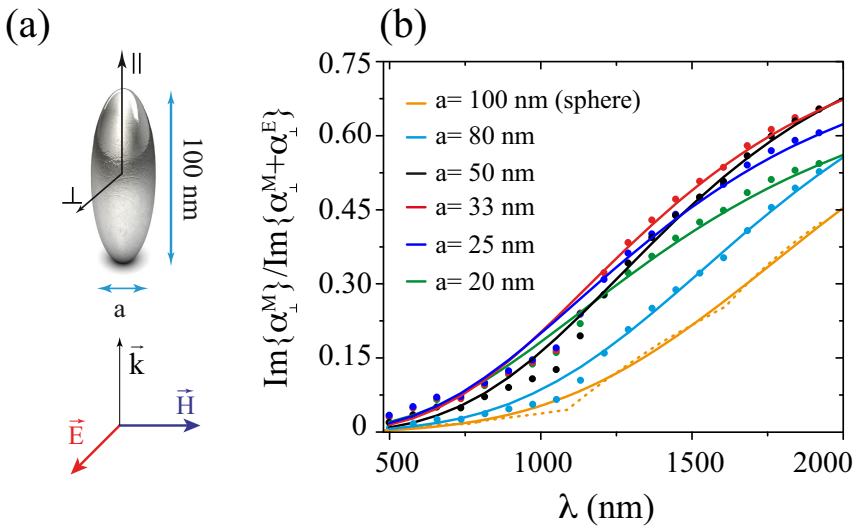

Fig. 8. Relative contribution of magnetic absorption for silver ellipsoids and light incidence along the axis of symmetry. (a) Sketch of the geometry. (b) Fraction of magnetic absorption. A Drude permittivity for silver is used in the solid curves and a tabulated dielectric function [27] for the dots.

Acknowledgments

We would like to thank Alberto G. Curto for useful discussions. This work has been supported in part by the Spanish MICINN (MAT2010-14885 and Consolider NanoLight.es) and the European Commission (FP7-ICT-2009-4-248909-LIMA and FP7-ICT-2009-4-248855-N4E). A. A.-G. and A. M. acknowledge financial support through FPU from the Spanish ME. V. M. acknowledges a CSIC - JAE grant.